catalysts

MDPI

Article

Photoelectrochemical Conversion of Sewage Water into H_2 Fuel over the $CuFeO_2$/CuO/Cu Composite Electrode

N. M. A. Hadia [1,2], Mohamed Shaban [3,4], Ashour M. Ahmed [4,5], W. S. Mohamed [1], Meshal Alzaid [1], Mohammed Ezzeldien [1], M. F. Hasaneen [1], Wassim El Malti [6,*], Ahmed Adel A. Abdelazeez [7] and Mohamed Rabia [4,8,*]

1 Physics Department, College of Science, Jouf University, Al-Jouf, Sakaka P.O. Box 2014, Saudi Arabia
2 Basic Sciences Research Unit, Jouf University, Sakaka 72388, Saudi Arabia
3 Department of Physics, Faculty of Science, Islamic University of Madinah, Prince Naifbin Abdulaziz, Al Jamiah, Madinah 42351, Saudi Arabia
4 Nanophotonics and Applications Laboratory, Physics Department, Faculty of Science, Beni-Suef University, Beni-Suef 62514, Egypt
5 Physics Department, College of Science, Imam Mohammad Ibn Saud Islamic University (IMSIU), Riyadh 11623, Saudi Arabia
6 College of Engineering and Technology, American University of the Middle East, Egaila 54200, Kuwait
7 Nanoscale Science Program, Department of Chemistry, University of North Carolina at Charlotte, Charlotte, NC 28223, USA
8 Nanomaterials Science Research Laboratory, Chemistry Department, Faculty of Science, Beni-Suef University, Beni-Suef 62514, Egypt
* Correspondence: wassim.elmalti@aum.edu.kw (W.E.M.); mohamedchem@science.bsu.edu.eg (M.R.)

Abstract: This study describes the synthesis of delafossite, $CuFeO_2$, as a primary photocatalytic material for hydrogen generation. A photoelectrode, $CuFeO_2$/CuO/Cu, was prepared by combusting a Cu foil dipped in $FeCl_3$ in ambient air. This photoelectrode showed excellent optical behavior for the hydrogen generation reaction from sewage water, producing 90 µmol/h of H_2. The chemical structure was confirmed through XRD and XPS analyses, and the crystalline rhombohedral shape of $CuFeO_2$ was confirmed using SEM and TEM analyses. With a bandgap of 1.35 ev, the prepared material displayed excellent optical properties. Electrochemical measurements for H_2 gas generation were carried out using the $CuFeO_2$/CuO/Cu photoelectrode, comparing the effect of light and dark and monochromatic wavelength light. The electrode exhibited significant enhancement in light compared to dark, with current density (J_{ph}) values of −0.83 and −0.1 mA.cm^{-2}, respectively. The monochromatic light also had a noticeable effect, with the J_{ph} value increasing from −0.45 to −0.79 mA·cm^{-2} as the wavelength increased from 640 to 390 nm. This system is cheap and durable, making it a promising solution for hydrogen gas fuel generation in the industry.

Keywords: delafossite; H_2 generation; photocatalyst; renewable energy; water splitting; SDG6; SDG7

Citation: Hadia, N.M.A.; Shaban, M.; Ahmed, A.M.; Mohamed, W.S.; Alzaid, M.; Ezzeldien, M.; Hasaneen, M.F.; El Malti, W.; Abdelazeez, A.A.A.; Rabia, M. Photoelectrochemical Conversion of Sewage Water into H_2 Fuel over the $CuFeO_2$/CuO/Cu Composite Electrode. *Catalysts* **2023**, *13*, 456. https://doi.org/10.3390/catal13030456

Academic Editors: Edward G. Gillan and Akira Nishimura

Received: 11 January 2023
Revised: 6 February 2023
Accepted: 14 February 2023
Published: 21 February 2023

1. Introduction

Renewable energy has become a vital energy source for people in today's society, as non-renewable energy sources are becoming scarce. Additionally, these energy sources are known to release dangerous gases, such as SOx, NOx, and COx, which can have adverse effects on the environment and human health [1–3].

Hydrogen gas (H_2) is a promising alternative energy source with numerous potential applications, including fuel for airplanes and factories and everyday household purposes such as cooking and heating. H_2 has a high combustion energy and low cost [4–7]. It can be produced through different electrolytes, such as strong acids or bases, by relying on the presence of high amounts of H^+ or OH^- ions through an extended mechanism that includes the formation of $OH^{\cdot}$. This active radical attacks the H_2O molecule for additional H_2 gas production. However, this reaction has limited economic applications related to the

cost of the chemicals, such as NaOH, HCl, or H_2SO_4, and the corrosion problems caused by the implemented electrolytes, affecting the working electrode.

The working electrode must be a semiconductor material, such as an oxide, sulfide, or nitride [8,9]. Oxides have the advantage of being cost-effective and stable [10,11]. Furthermore, the amount of the produced H_2 gas depends on the optical and morphological properties of the semiconductor material, making it crucial to prepare these materials with high surface areas and active sites [12–14]. One of the developed methods for increasing H_2 production is using plasmonic materials in the electrode construction; copper (Cu) is a promising and cost-effective plasmonic material [15,16]. In the literature, several studies have used Cu as plasmonic material to increase the activity of ZnO as a photocatalytic material [17]. Plasmonic materials enhance the performance of the neighboring semiconductor material (such as a metal oxide) by transferring electrons to the conducting band and inducing a plasmonic resonance that generates an electric field and increases light absorbance [18].

The physical properties of the prepared photocatalytic material play a crucial role in improving the light absorbance and reducing the bandgap. Copper oxide (CuO), with its black color and semiconducting nature, has a bandgap of 0.7 to 1.6 eV, which falls within the visible light absorbance region [19,20]. This behavior enhances its application as a photocatalytic absorbent and in H_2 production [21,22]. Li et al. synthesized CuO/Cu through annealing $Cu(OH)_2$ in air conditions at 500 °C [23]. Moreover, Sagadevan et al. synthesized CuO through the combustion process using ascorbic acid as a capping agent at 100–300 °C [24]. Ragupathi et al. synthesized CuO supported with b-C_3N_4 as photocatalytic material for water splitting reaction; the produced J_{ph} is still very small [25]. Quyen et al. increased the efficiency of the H_2 generation of TiO_2 by using Cu nanomaterials as plasmonic material [26]. In the same manner, Shen et al. slightly increased H_2 generation when g-C_3N_4 was decorated with CuO, but not to the extent desired [27].

Delafossite, $CuFeO_2$, has a high photocatalytic performance and excellent optical properties, with a bandgap of approximately 1.3 eV [28]. This material can be prepared using various methods, including solvothermal and laser beam techniques. He et al. used $CuFeO_2$ for carbamazepine degradation with an efficiency of 86% [29]. In addition, $GC_3N_4/CuFeO_2$ has been used as a catalyst for H_2O_2 degradation through the Fenton reaction [30]. Mao et al. prepared $CuFeO_2$ using the hydrothermal and solar gel for dye removal and water splitting, and the obtained J_{ph} was recorded as 4×10^{-6} μA cm^{-2} in 1M NaOH [31]. Baiano et al. investigated the significant photocatalytic reduction of CO_2 utilizing $CuFeO_2$ through DFT calculations [32]. Furthermore, $CuFeO_2$ was demonstrated to have photocatalytic antibacterial properties, effectively degrading *E. coli*, with an improvement in performance when exposed to light [33]. Change et al. used Mg-doped $CuFeO_2$ for photocatalytic degradation of methylene blue and reduction of CO_2 to form ethylene glycol under the electrolysis conditions [34].

In the previous studies on H_2 generation, the use of additional electrolytes such as HCl or NaOH was required to serve as a source of H^+ ions [35–37]. Additionally, some studies relied on high-cost preparation techniques [38,39].

In this study, a $CuFeO_2/CuO$ delafossite material was synthesized on a Cu metal substrate through a combustion reaction. Subsequently, various analyses were performed to confirm the chemical, optical, and morphological properties of the prepared photoelectrode, $CuFeO_2/CuO/Cu$. The latter was then evaluated for its ability to produce H_2 gas through photocatalytic decomposition of sewage water, and the effects of light and dark conditions on H_2 production were investigated. The impact of different monochromatic wavelengths on H_2 production was also examined, and the amount of H_2 produced was calculated over time.

2. Results and Discussion

2.1. Characterization of $CuFeO_2/CuO/Cu$ Nanomaterials Photoelectrode

The XRD analysis was employed to investigate and verify the crystalline structure of the prepared $CuFeO_2/CuO/Cu$ nanomaterials. The results showed a well-demonstrated rhombohedral $CuFeO_2$ phase structure and microstructural parameters of the prepared

nanostructured electrode. Figure 1a displays the XRD patterns of the prepared $CuFeO_2$, which show a poly-oriented nature. Fifteen diffraction peaks were observed; eleven of the peaks correspond to the Miller indices (i.e., (*hkl*) planes) (006), (101), (012),(104), (009), (018), (110), (1010), (116), (202), and (024) of the rhombohedral $CuFeO_2$ structure with a secondary CuO impurity phase. The remaining four peaks correspond to the Miller indices (112), (020), (202), and (311) of the CuO monoclinic phase. The peaks are in agreement with the reference data JCPDS 01-075-2146 [40] for the rhombohedral structure of pure $CuFeO_2$ with $R-3\,m$ space group and JCPDS card no. 48-1548 [41] for the monoclinic phase of CuO.

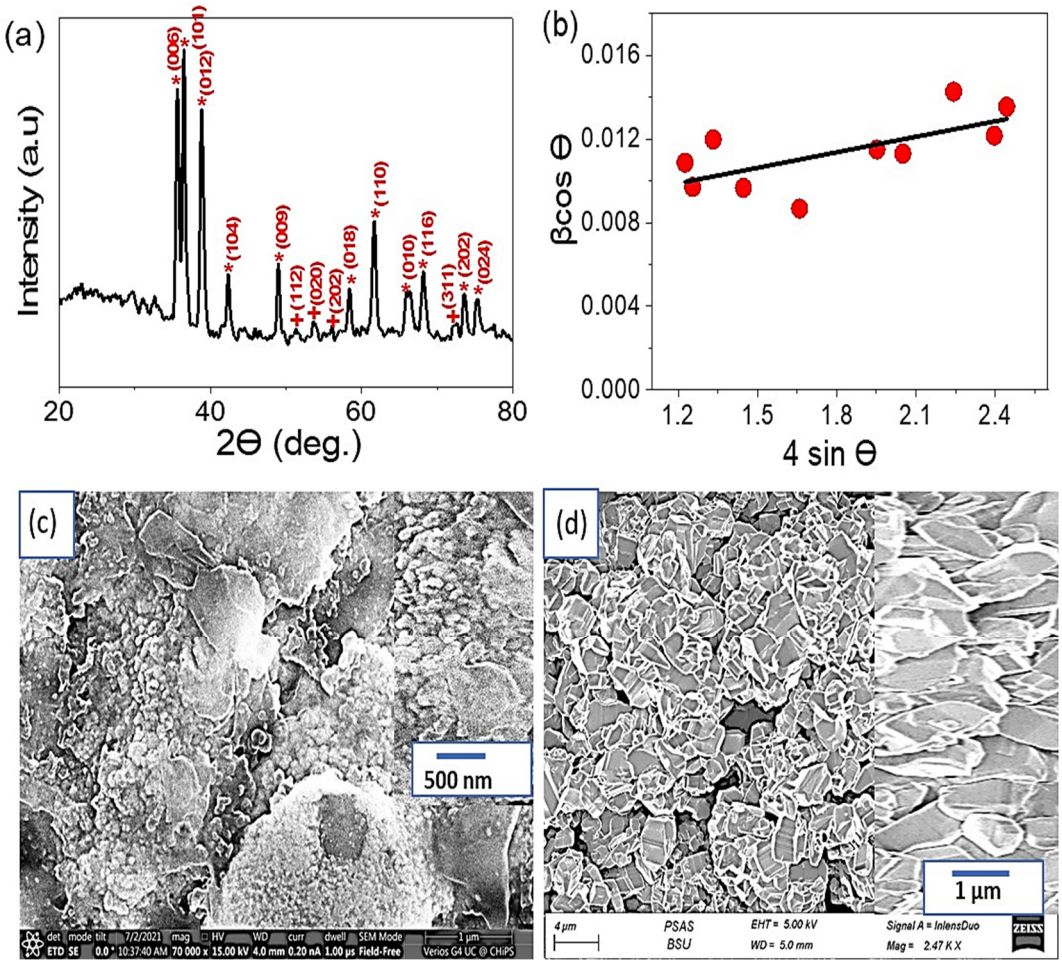

Figure 1. (**a**) XRD patterns and (**b**) W–H plots of $CuFeO_2$. (**c**) SEM of CuO and (**d**) $CuFeO_2$ nanomaterial.

The broadness of the XRD patterns was exploited to estimate the microstructural parameters, such as crystallite size (D) and microstrain (ε), of the prepared $CuFeO_2$ by using the Williamson–Hall (W–H) approach. The W-H model was applied to the pure peak broadening of the diffraction peaks to calculate the mean values of (D) and (ε). The pure peak broadening (β) was obtained from (Equation (1)) [42–44]

$$\beta \quad \cos\theta = \frac{0.95\,\lambda}{D} + 4\varepsilon \quad \sin\theta \tag{1}$$

Where 0.95 is the shape factor value for $CuFeO_2$ nanoparticles, and λ is the incident XRD wavelength (~0.15418 nm). In Equation (1), it was considered that the investigated samples have an isotropic nature, and the micro-strain is uniform in all (*hkl*) crystallographic directions. The crystallite size (D) and the micro-strain (ε) values were estimated by plotting the ($\beta_{Correct}$ cos θ) versus (4 sin θ) for each XRD peak, yielding a linear regression where

the intercept and slope were calculated (Figure 1b). It was found that the crystalline size and micro-strain values for the $CuFeO_2$ sample are 35 nm and 4.69×10^{-3}, respectively.

Moreover, the XRD of the CuO nanoparticles is provided in Figure S1; the peaks appearing at $2\theta^\circ$ = 26.55, 35.27, and 41.71° correspond to CuO for the growth direction (110), (111), and (200), respectively. These analyses match the results reported in the literature [45–47]. On the other hand, the Cu metal appears at 43.5°, 50.7°, and 74.5° [46,48].

XPS was utilized for further verification of the chemical composition of $CuFeO_2$. The results are presented in Figure S2a, in which Cu, Fe, and O elements are confirmed through their related peaks. Additionally, the spectra of the Cu_{2p} spin-orbital components reveal six peaks in the range of 930 to 970 eV, as shown in Figure S2b. The Fe_{2P} spectra are confirmed through the two peaks at 723 and 726 eV (Figure S2c). The O_{1s} spin-orbital peaks can be found in the 529–533 eV range (Figure S2d).

In Figure 1c, The morphology of CuO can be clearly seen as protruding appendages that greatly enhance the surface area. The magnified image shows that the appendages are randomly distributed across the surface. After forming $CuFeO_2$ (Figure 1d), excellent uniform crystalline rhombohedral shapes appear with porous structure. This highly crystalline structure confirms the findings of the XRD analysis. Given the crystalline nature of the prepared materials, it was expected that their optical properties would be superior [49].

The optical reflectance of $CuFeO_2$ nanoparticles was determined over the wavelength range of 200 to 1200 nm, as shown in Figure 2a. The low reflectance of the $CuFeO_2$ nanoparticles in the visible region confirms their high absorbance in the UV and IR regions. The bandgap of the material was calculated using the Kubelka-Munk equation (Equation (2)) [12], which takes into account reflectance (R), with K and S values that represent the molar absorption coefficient and scattering factor, respectively. The resulting bandgap of this material is 1.35 eV.

$$K/S = \frac{(1-R)^2}{2R}. \quad (2)$$

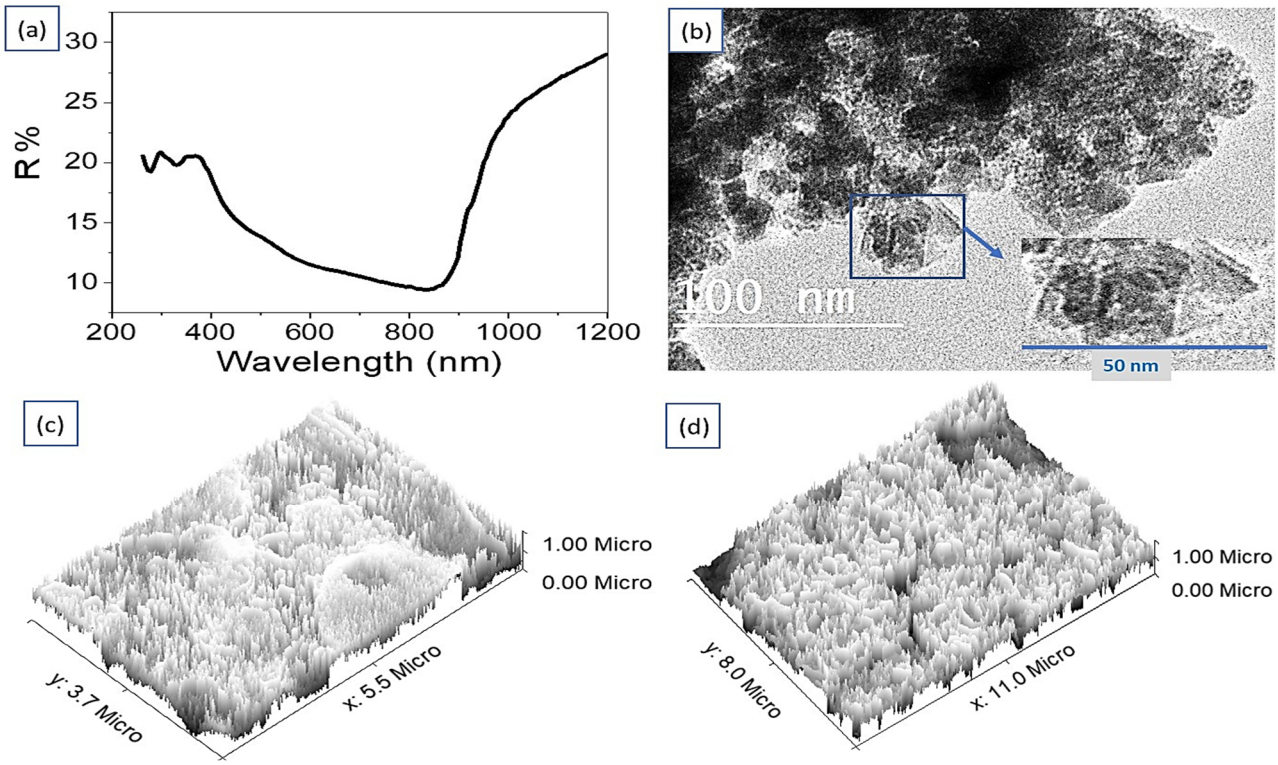

Figure 2. (**a**) The optical reflectance and (**b**) TEM of $CuFeO_2$. ImageJ theoretical of (**c**) CuO and (**d**) $CuFeO_2$ nanoparticles.

The TEM image of $CuFeO_2$ is displayed in Figure 2b, which confirms the formation of crystalline nanoparticles with an average size of 50 nm. These results are consistent with those obtained from the SEM analysis. The theoretical images of CuO and $CuFeO_2$, obtained using ImageJ, are presented Figure 2c,d, respectively. Both materials exhibit considerable roughness, but the roughness of the $CuFeO_2$ is more uniform. This feature indicates the suitability of these materials for photocatalytic applications due to their high ability to capture light through their porous structures, acting like a "cave" for the incident photons [3,12].

2.2. Photoelectrochemical Water Splitting

The photoelectrochemical water splitting reaction was carried out with a three-electrode cell. The prepared $CuFeO_2/CuO/Cu$ photoelectrode served as the working electrode, graphite as the counter electrode, and calomel as the reference electrode. The measurements were conducted using a CHMI608E electrochemical workstation under a 400 W metal halide lamp at a sweep rate of 1 mV/s and a temperature of 25 °C. The measurements were taken both in the dark and under illumination to assess the photocatalytic behavior of the materials.

The impact of light on the performance of $CuFeO_2/CuO/Cu$ is depicted in Figure 3a. When illuminated, the current density (J_{ph}) value was increased; the J_{ph} values at 0.88 V in dark and light conditions were -0.10 mA·cm^{-2} and -0.83 mA·cm^{-2}, respectively. The high surface area of the $CuFeO_2/CuO/Cu$ provides a good environment for capturing photons, which leads to the creation of electron-hole pairs. The electrons collected on the surface of $CuFeO_2$ are then transferred to the adjacent electrolyte (sewage water), leading to further reactions and the generation of OH· radicals. The results of this study show that using sewage water as an electrolyte (pH 7.2) is a promising approach, as its chemical composition, outlined in Table 1, acts as a catalyst for the water-splitting reaction.

The addition of Cu increased the efficiency of electron transfer. It also acts as a plasmonic material that enhances light capture, causing an electric field to accumulate around the $CuFeO_2$ materials. This electric field oscillation between Cu and $CuFeO_2$ increases the number of free electrons available to split water into H_2 gas. The rate of H_2 gas released can be determined from the calculated J_{ph} values.

The H_2 production was measured and plotted in Figure 3b. It was found that the H_2 production increased with time, reaching 90 µmol/h. This high rate confirms the effectiveness of $CuFeO_2$ as a photocatalyst in water splitting. The active sites of $CuFeO_2$ are activated under light, contributing to its high efficiency. Based on Equation (3), the number of photons was estimated to be 8×10^{21} photon/s, which leads to a significant number of electrons being generated and collected on the active sites, and then transferred to the neighbor electrolyte for further water splitting and H_2 gas production [50,51]. λ, h, P, and c in Equation (3) are wavelength, Planck constant, light intensity, and light velocity, respectively.

The number of generated H_2 moles was determined using Faraday's law (Equation (4)) [52,53]. This calculation is based on the time change (dt) and the J_{ph} values, with consideration given to the Faraday constant (F).

$$N = \lambda P/hc \tag{3}$$

$$H_2 \text{ mole} = \int_0^t J_{ph} \cdot dt/F \tag{4}$$

The performance of the prepared $CuFeO_2/CuO/Cu$ photoelectrode was evaluated under monochromatic light by studying the effect of different light wavelengths (390–640 nm) on the H_2 generation reaction. The results, presented in Figure 4a, show that the J_{ph} values increased from -0.45 to -0.79 mA·cm^{-2} as the wavelength increased from 390 to 640 nm. Figure 4b shows the produced J_{ph} values at -0.88 V, confirming that the sewage water splitting and H_2 gas evolution reactions were enhanced with increasing incident photons.

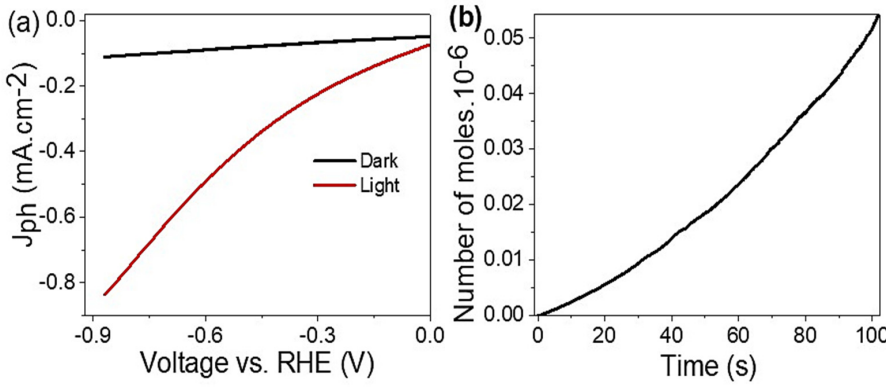

Figure 3. (**a**) The voltage-current relation in dark and light and (**b**) the H_2 moles produced vs. time for the $CuFeO_2/CuO/Cu$ photoelectrode.

Table 1. The chemical composition of the sewage water used as an electrolyte for H_2 gas production.

Species	Concentration (mg/L)
Phenols	0.015
F^-	1.0
Al^{3+}	3.0
NH_3	5.0
Hg^{2+}	0.005
Pb^{2+}	0.5
Cd^{3+}	0.05
As^{3+}	0.05
Cr^{3+}	1.0
Cu^{2+}	1.5
Ni^{3+}	0.1
Fe^{3+}	1.5
Mn^{2+}	1.0
Zn^{2+}	5.0
Ag^+	0.1
Ba^{3+}	2.0
Co^{2+}	2.0
Other cations	0.1
Pesticides	0.2
CN^{-1}	0.1
Industrial washing	0.5
Coli groups	400

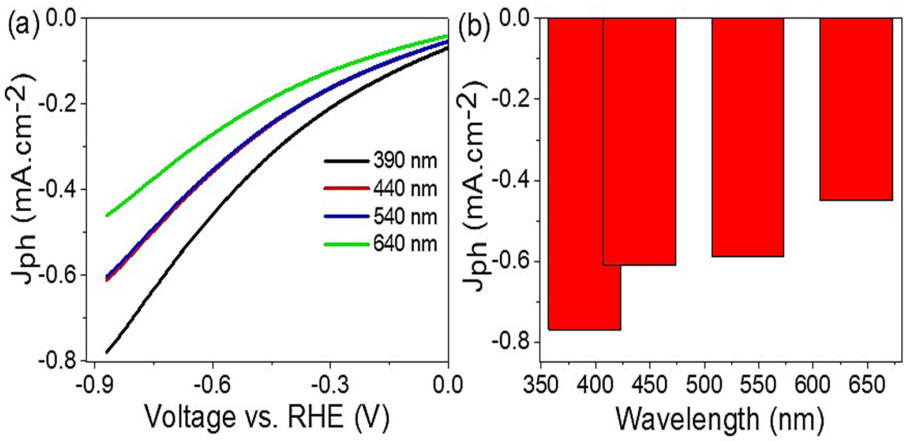

Figure 4. (**a**) The effect of monochromatic wavelengths on the prepared $CuFeO_2/CuO/Cu$ photoelectrode and (**b**) the produced J_{ph} values at −0.88 V.

The conversion of sewage water into H_2 gas was achieved through the impact of the incident photons on the $CuFeO_2/CuO/Cu$ photoelectrode. The Delafossite material is highly responsive to light illumination, which activates the surface and triggers energy level splitting. Hot electrons are then collected on the surface and transferred to the upper level through resonance energy transfer. The small bandgap, 1.35 eV, is considered promising for electron transfer and confirms the significant optical properties of this material, as seen Figure 2a. The use of Cu as a current collector facilitates this electron transfer process as it can also act as a plasmonic material [52]. The collected electrons are then transferred to the surrounding wastewater solution, generating the current density (J_{ph}) values shown in Figure 3. These J_{ph} values determine the rate of H_2 gas produced [51,54,55]. The photocurrent is recorded as -0.11 mA·cm^{-2}. The generation of H_2 is initiated by the radiation of light that creates electrons and holes, leading to hot electrons being transferred to the photocathode for reduction and, eventually, H_2 production [56].

The *IPCE* of the photoelectrode, $CuFeO_2/CuO/Cu$, is determined through Equation (5) and found to be 2.4% at 340 nm, which is a favorable result for producing hydrogen from a solution without using additional electrolytes [57].

$$IPCE = \frac{J_{ph}\left(mA \cdot cm^{-2}\right) \cdot 1240\ (V \cdot nm)}{P(mW \cdot cm^{-2}) \cdot \lambda(nm)} \quad (5)$$

Finally, a comparison was made between the electrolytes used and the produced J_{ph} values in the literature and those obtained in this study, where sewage water was used as an electrolyte. The results are summarized in Table 2 and show that the $CuFeO_2/CuO/Cu$ electrode prepared in this study has one of the highest J_{ph} values, indicating its high efficiency and sensitivity to light. Furthermore, this study's results are noteworthy as sewage water was used as the electrolyte without needing additional external electrolytes, making it a significant advantage over other electrodes.

Table 2. Comparison of the current study (using sewage water as an electrolyte) with the previous studies in the literature [58].

Photoelectrode	Electrolyte	J_{ph} (mA/cm^2)
g-C_3N_4-CuO [25]	NaOH	0.01
CuO-C/TiO_2 [59]	Glycerol	0.012
SnO_2/TiO_2 [60]	$Na_2S_2O_3$	0.4
TiN-TiO_2 [61]	NaOH	3.0×10^{-4}
$BiFeO_3$ [62]	NaOH	0.1
Au/Pb(Zr, Ti)O_3 [63]	NaOH	0.06
PrFeO [64]	Na_2SO_4	0.130
Poly(3-aminobenzoic acid) frame [65]	H_2SO_4	0.08
$CuFeO_2/CuO/Cu$ (present study)	Sewage water	0.83

3. Materials and Methods

3.1. $CuFeO_2$ Delafossite Nanomaterial Preparation

The $CuFeO_2$ nanomaterial was prepared through a simple combustion reaction. The process began with washing the Cu foil with water, soap, distilled water, and ethanol, followed by immersing it in concentrated H_2SO_4 (99.9%) for 2–3 min. The foil was then rewashed with distilled water and ethanol. Subsequently, it was immersed in 0.05 M $FeCl_3$ for 15 min on each side and dried at 60 °C for 2 h. The final step involved combusting the substrate at 500 °C for 10 min, forming the $CuFeO_2/CuO/Cu$ photoelectrode.

3.2. Characterization

The prepared $CuFeO_2$ materials were characterized using various analysis methods. The chemical structure was examined by x-ray diffraction patterns (XRD, Malvern Panalytical Ltd., Malvern, UK) (λ = 0.15418 nm) (advance diffractometer, Bruker D8) and X-ray photoelectron spectroscopy (XPS, K-ALPHA, Waltham, MA, USA). The morphology was

observed by scanning electron microscopy (SEM, S-4800, Hitachi, Japan) and transmitted electron microscopy (TEM, JEOL JEM-2100, Oberkochen, Germany). Finally, the optical properties were analyzed using a double-beam spectrophotometer (Elmer Lamba, Waltham, MA, USA).

3.3. Electrochemical Measurements

The electrochemical measurements were performed using a CHI608E electrochemical workstation, as illustrated in Figure 5. The prepared $CuFeO_2/CuO/Cu$ photoelectrode served as the working electrode (1 cm^2), while a calomel and graphite electrodes were used as the reference and counter electrodes, respectively. The measurements were carried out using sewage water with a pH of 7.2. A 400 W metal halide lamp (light intensity) with a photon flux of 500 µmol/s was implemented as the light source. The effect of different light wavelengths (390, 440, 540, and 640 nm) and the impact of alternating light and dark conditions were studied. The produced H_2 moles were calculated as a function of time.

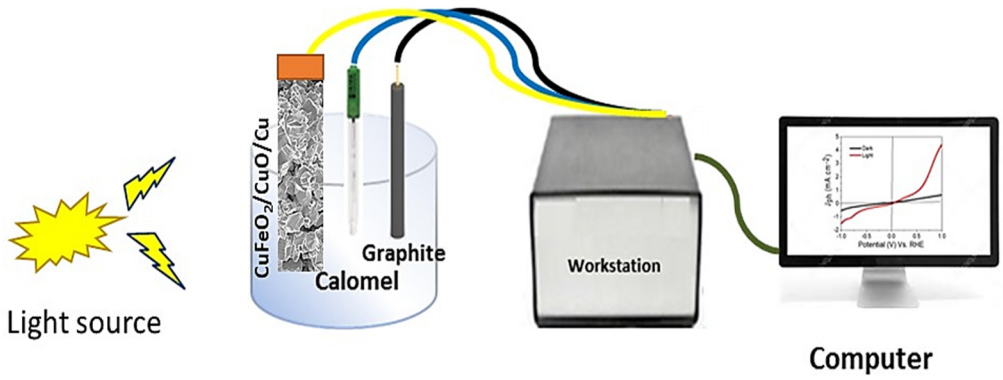

Figure 5. The schematic diagram for the H_2 generation from sewage water, using the $CuFeO_2/CuO/Cu$ photoelectrode.

4. Conclusions

This study demonstrates the potential of a low-cost photoelectrode made of $CuFeO_2/CuO/Cu$ for the generation of H_2 gas. Using sewage water as an electrolyte, measurements were conducted using an electrochemical workstation in a three-electrode cell setup. The photoelectrode was found to have excellent optical properties, with a small bandgap of 1.35 eV, making it suitable for photocatalytic reactions. The electrochemical testing under a metal halide lamp was applied; the results showed that the J_{ph} values under light and dark conditions were −0.83 and −0.1 $mA{\cdot}cm^{-2}$, respectively. The effect of monochromatic light on the photoelectrode was studied across the range of 390 to 640 nm, resulting in J_{ph} values of −0.45 to −0.79 $mA{\cdot}cm^{-2}$. The produced H_2 gas was measured to be 90 µmol/h. Additionally, the cost of a 10 × 10 cm^2 $CuFeO_2/CuO/Cu$ photoelectrode was found to be 0.5 $, making it a cost-effective option for H_2 gas production and a candidate for industrial applications.

Supplementary Materials: The following supporting information can be downloaded at: https://www.mdpi.com/article/10.3390/catal13030456/s1, Figure S1: XRD of the CuO nanoparticles. and Figure S2: XPS (a) survey, (b) Cu, (c) Fe, and (d) O elements for the synthesized $CuFeO_2$ nano-material.

Author Contributions: Conceptualization, N.M.A.H., M.S., and M.R.; methodology, N.M.A.H., W.S.M., M.A., M.E., M.F.H., M.S., A.M.A., and M.R.; validation, formal analysis, data curation, N.M.A.H., W.S.M., M.A., M.E., M.F.H., M.S., A.M.A., W.E.M., and M.R.; software, investigation, A.A.A.A., M.S., and M.R.; writing—original draft preparation, writing—review and editing, visualization, W.E.M. and M.R.; supervision, project administration, resources, funding acquisition, N.M.A.H. and M.R. All authors have read and agreed to the published version of the manuscript.

Funding: This research received no external funding.

Data Availability Statement: The data that support the findings of this study are available from the corresponding author upon reasonable request.

Acknowledgments: The authors extend their appreciation to the Deanship of Scientific Research at Jouf University for funding this work through research grant no. (DSR2022-GR-0122).

Conflicts of Interest: The authors declare no conflict of interest.

References

1. Mohamed, F.; Rabia, M.; Shaban, M. Synthesis and Characterization of Biogenic Iron Oxides of Different Nanomorphologies from Pomegranate Peels for Efficient Solar Hydrogen Production. *J. Mater. Res. Technol.* **2020**, *9*, 4255–4271. [CrossRef]
2. Shaban, M.; Ali, S.; Rabia, M. Design and Application of Nanoporous Graphene Oxide Film for CO_2, H_2, and C_2H_2 Gases Sensing. *J. Mater. Res. Technol.* **2019**, *8*, 4510–4520. [CrossRef]
3. Elsayed, A.M.; Rabia, M.; Shaban, M.; Aly, A.H.; Ahmed, A.M. Preparation of Hexagonal Nanoporous Al_2O_3/TiO_2/TiN as a Novel Photodetector with High Efficiency. *Sci. Rep.* **2021**, *11*, 17572. [CrossRef]
4. Nishiyama, H.; Yamada, T.; Nakabayashi, M.; Maehara, Y.; Yamaguchi, M.; Kuromiya, Y.; Nagatsuma, Y.; Tokudome, H.; Akiyama, S.; Watanabe, T.; et al. Photocatalytic Solar Hydrogen Production from Water on a 100-M^2 Scale. *Nature* **2021**, *598*, 304–307. [CrossRef] [PubMed]
5. Hisatomi, K.D.T. Reaction Systems for Solar Hydrogen Production via Water Splitting with Particulate Semiconductor. *Nat. Catal.* **2019**, *2*, 387–399. [CrossRef]
6. Pagliaro, M. Preparing for the Future: Solar Energy and Bioeconomy in the United Arab Emirates. *Energy Sci. Eng.* **2019**, *7*, 1451–1457. [CrossRef]
7. Takata, T. Photocatalytic Water Splitting with Quantum Efficiency of Almost Unity. *Nature* **2020**, *581*, 411–414. [CrossRef] [PubMed]
8. Kang, Z.; Cheng, Y.; Zheng, Z.; Cheng, F.; Chen, Z.; Li, L.; Tan, X.; Xiong, L.; Zhai, T.; Gao, Y. MoS2-Based Photodetectors Powered by Asymmetric Contact Structure with Large Work Function Difference. *Nano-Micro Lett.* **2019**, *11*, 34. [CrossRef]
9. Lee, J.H.; Lee, W.W.; Yang, D.W.; Chang, W.J.; Kwon, S.S.; Park, W. Il Anomalous Photovoltaic Response of Graphene-on-GaN Schottky Photodiodes. *ACS Appl. Mater. Interfaces* **2018**, *10*, 14170–14174. [CrossRef]
10. Shaban, M.; Rabia, M.; El-Sayed, A.M.A.; Ahmed, A.; Sayed, S. Photocatalytic Properties of PbS/Graphene Oxide/Polyaniline Electrode for Hydrogen Generation. *Sci. Rep.* **2017**, *7*, 14100. [CrossRef]
11. Rabia, M.; Mohamed, H.S.H.; Shaban, M.; Taha, S. Preparation of Polyaniline/PbS Core-Shell Nano/Microcomposite and Its Application for Photocatalytic H_2 Electrogeneration from H_2O. *Sci. Rep.* **2018**, *8*, 1107. [CrossRef] [PubMed]
12. Mohamed, H.S.H.; Rabia, M.; Zhou, X.G.; Qin, X.S.; Khabiri, G.; Shaban, M.; Younus, H.A.; Taha, S.; Hu, Z.Y.; Liu, J.; et al. Phase-Junction Ag/TiO_2 Nanocomposite as Photocathode for H_2 Generation. *J. Mater. Sci. Technol.* **2021**, *83*, 179–187. [CrossRef]
13. Rabia, M.; Shaban, M.; Jibali, B.M.; Abdelkhaliek, A.A. Effect of Annealing Temperature on the Photoactivity of ITO/VO_2 (M)/Au Film Electrodes for Water Splitting. *J. Nanosci. Nanotechnol.* **2020**, *20*, 4120–4130. [CrossRef] [PubMed]
14. Rabia, M.; Mohamed, S.H.; Zhao, H.; Shaban, M.; Lei, Y.; Ahmed, A.M. TiO_2/TiOxNY Hollow Mushrooms-like Nanocomposite Photoanode for Hydrogen Electrogeneration. *J. Porous Mater.* **2020**, *27*, 133–139. [CrossRef]
15. Zhang, X.; Li, J.; Yang, W.; Leng, B.; Niu, P.; Jiang, X.; Liu, B. High-Performance Flexible Ultraviolet Photodetectors Based on AZO/ZnO/PVK/PEDOT:PSS Heterostructures Integrated on Human Hair. *ACS Appl. Mater. Interfaces* **2019**, *11*, 24459–24467. [CrossRef] [PubMed]
16. Kim, J.; Lee, H.C.; Kim, K.H.; Hwang, M.S.; Park, J.S.; Lee, J.M.; So, J.P.; Choi, J.H.; Kwon, S.H.; Barrelet, C.J.; et al. Photon-Triggered Nanowire Transistors. *Nat. Nanotechnol.* **2017**, *12*, 963–968. [CrossRef]
17. Li, M.; Yu, M.; Su, D.; Zhang, J.; Jiang, S.; Wu, J.; Wang, Q.; Liu, S. Ultrahigh Responsivity UV Photodetector Based on Cu Nanostructure/ZnO QD Hybrid Architectures. *Small* **2019**, *15*, 1901606. [CrossRef]
18. Almohammedi, A.; Shaban, M.; Mostafa, H.; Rabia, M. Nanoporous TiN/TiO_2/Alumina Membrane for Photoelectrochemical Hydrogen Production from Sewage Water. *Nanomaterials* **2021**, *11*, 2617. [CrossRef]
19. Schultze, J.W.; Lohrengel, M.M. Stability, Reactivity and Breakdown of Passive Films. Problems of Recent and Future Research. *Electrochim. Acta* **2000**, *45*, 2499–2513. [CrossRef]
20. Basnet, P.; Zhao, Y. Tuning the CuxO Nanorod Composition for Efficient Visible Light Induced Photocatalysis. *Catal. Sci. Technol.* **2016**, *6*, 2228–2238. [CrossRef]
21. Chiang, C.Y.; Shin, Y.; Aroh, K.; Ehrman, S. Copper Oxide Photocathodes Prepared by a Solution Based Process. *Int. J. Hydrogen Energy* **2012**, *37*, 8232–8239. [CrossRef]
22. Chiang, C.-Y.; Chang, M.-H.; Liu, H.-S.; Tai, C.Y.; Ehrman, S. Process Intensification in the Production of Photocatalysts for Solar Hydrogen Generation. *Ind. Eng. Chem. Res.* **2012**, *51*, 5207–5215. [CrossRef]
23. Li, C.; Kurniawan, M.; Sun, D.; Tabata, H.; Delaunay, J.J. Nanoporous CuO Layer Modified Cu Electrode for High Performance Enzymatic and Non-Enzymatic Glucose Sensing. *Nanot* **2015**, *26*, 015503. [CrossRef]
24. Sagadevan, S.; Vennila, S.; Marlinda, A.R.; Al-Douri, Y.; Rafie Johan, M.; Anita Lett, J. Synthesis and Evaluation of the Structural, Optical, and Antibacterial Properties of Copper Oxide Nanoparticles. *Appl. Phys. A Mater. Sci. Process.* **2019**, *125*, 489. [CrossRef]
25. Ragupathi, V.; Raja, M.A.; Panigrahi, P.; Ganapathi Subramaniam, N. CuO/g-C_3N_4 Nanocomposite as Promising Photocatalyst for Photoelectrochemical Water Splitting. *Optik* **2020**, *208*, 164569. [CrossRef]

26. Thi Quyen, V.; Jitae, K.; Thi Huong, P.; Thi Thu Ha, L.; My Thanh, D.; Minh Viet, N.; Quang Thang, P. Copper Doped Titanium Dioxide as a Low-Cost Visible Light Photocatalyst for Water Splitting. *Sol. Energy* **2021**, *218*, 150–156. [CrossRef]
27. Chen, J.; Shen, S.; Guo, P.; Wang, M.; Wu, P.; Wang, X.; Guo, L. In-Situ Reduction Synthesis of Nano-Sized Cu_2O Particles Modifying g-C_3N_4 for Enhanced Photocatalytic Hydrogen Production. *Appl. Catal. B Environ.* **2014**, *152–153*, 335–341. [CrossRef]
28. Liu, Q.L.; Zhao, Z.Y.; Zhao, R.D.; Yi, J.H. Fundamental Properties of Delafossite $CuFeO_2$ as Photocatalyst for Solar Energy Conversion. *J. Alloys Compd.* **2020**, *819*, 153032. [CrossRef]
29. He, B.; Zhao, Z.; Song, L.; Liu, W.; Yang, Y.; Shang, J.; Cheng, X. Highly Efficient Activation of Peroxymonosulfate by the (3R + 2H)-$CuFeO_2$ Nanocomposite Photocatalyst: Intermediate Toxicity, BVS Validation Ionic Migration and Degradation Pathway. *Sep. Purif. Technol.* **2022**, *289*, 120729. [CrossRef]
30. Dai, C.; Nie, Y.; Tian, X.; Yang, C.; Hu, Y.; Lin, H.M.; Dionysiou, D.D. Insight into Enhanced Fenton-like Degradation of Antibiotics over $CuFeO_2$ Based Nanocomposite: To Improve the Utilization Efficiency of OH/O $_2$- via Minimizing Its Migration Distance. *Chemosphere* **2022**, *294*, 133743. [CrossRef]
31. Mao, L.; Mohan, S.; Gupta, S.K.; Mao, Y. Multifunctional Delafossite $CuFeO_2$ as Water Splitting Catalyst and Rhodamine B Sensor. *Mater. Chem. Phys.* **2022**, *278*, 125643. [CrossRef]
32. Baiano, C.; Schiavo, E.; Gerbaldi, C.; Bella, F.; Meligrana, G.; Talarico, G.; Maddalena, P.; Pavone, M.; Muñoz-García, A.B. Role of Surface Defects in CO_2 Adsorption and Activation on $CuFeO_2$ Delafossite Oxide. *Mol. Catal.* **2020**, *496*, 111181. [CrossRef]
33. Nien, Y.T.; Chen, Y.Z.; Hsu, Y.R.; Ye, H.J. Enhanced Antibacterial Effect of $CuFeO_2$ Ceramic Powders by Glycine Combustion Process and Visible Light Irradiation. *Mater. Chem. Phys.* **2022**, *276*, 125423. [CrossRef]
34. Chang, Y.H.; Wang, H.; Siao, T.F.; Lee, Y.H.; Bai, S.Y.; Liao, C.W.; Zhuang, J.K.; Chiu, T.W.; Kuo, C.H. A New Solution Route for the Synthesis of $CuFeO_2$ and Mg-Doped $CuFeO_2$ as Catalysts for Dye Degradation and CO_2 Conversion. *J. Alloys Compd.* **2021**, *854*, 157235. [CrossRef]
35. Teixeira, G.F.; Silva Junior, E.; Vilela, R.; Zaghete, M.A.; Colmati, F. Perovskite Structure Associated with Precious Metals: Influence on Heterogenous Catalytic Process. *Catalysts* **2019**, *9*, 721. [CrossRef]
36. Mishra, M.; Chun, D.M. α-Fe_2O_3 as a Photocatalytic Material: A Review. *Appl. Catal. A Gen.* **2015**, *498*, 126–141. [CrossRef]
37. Acar, C.; Dincer, I.; Naterer, G.F. Review of Photocatalytic Water-Splitting Methods for Sustainable Hydrogen Production. *Int. J. Energy Res.* **2016**, *40*, 1449–1473. [CrossRef]
38. Chiang, C.Y.; Aroh, K.; Franson, N.; Satsangi, V.R.; Dass, S.; Ehrman, S. Copper Oxide Nanoparticle Made by Flame Spray Pyrolysis for Photoelectrochemical Water Splitting—Part II. Photoelectrochemical Study. *Int. J. Hydrogen Energy* **2011**, *36*, 15519–15526. [CrossRef]
39. Guo, X.; Diao, P.; Xu, D.; Huang, S.; Yang, Y.; Jin, T.; Wu, Q.; Xiang, M.; Zhang, M. CuO/Pd Composite Photocathodes for Photoelectrochemical Hydrogen Evolution Reaction. *Int. J. Hydrogen Energy* **2014**, *39*, 7686–7696. [CrossRef]
40. Cheng, X.; Ding, J.; Wu, Y.; Liu, H.; Dawson, G. The Photocathodic Properties of a Fe_2O_3 Wrapped $CuFeO_2$ Layer on ITO Glass for Water Splitting. *Chem. Phys.* **2018**, *513*, 241–245. [CrossRef]
41. Siddiqui, H.; Parra, M.R.; Qureshi, M.S.; Malik, M.M.; Haque, F.Z. Studies of Structural, Optical, and Electrical Properties Associated with Defects in Sodium-Doped Copper Oxide (CuO/Na) Nanostructures. *J. Mater. Sci.* **2018**, *53*, 8826–8843. [CrossRef]
42. Mohamed, W.S.; Alzaid, M.; Abdelbaky, M.S.M.; Amghouz, Z.; García-Granda, S.; Abu-Dief, A.M. Impact of Co^{2+} Substitution on Microstructure and Magnetic Properties of $Co_xZn_{1-X}Fe_2O_4$ Nanoparticles. *Nanomaterials* **2019**, *9*, 1602. [CrossRef]
43. Mohamed, W.S.; Hadia, N.M.A.; Al Bakheet, B.; Alzaid, M.; Abu-Dief, A.M. Impact of Cu^{2+} Cations Substitution on Structural, Morphological, Optical and Magnetic Properties of $Co_{1-X}Cu_xFe_2O_4$ Nanoparticles Synthesized by a Facile Hydrothermal Approach. *Solid State Sci.* **2022**, *125*, 106841. [CrossRef]
44. Mohamed, W.S.; Abu-Dief, A.M. Impact of Rare Earth Europium (RE-Eu^{3+}) Ions Substitution on Microstructural, Optical and Magnetic Properties of $CoFe_{2-x}Eu_xO_4$ Nanosystems. *Ceram. Int.* **2020**, *46*, 16196–16209. [CrossRef]
45. Zúñiga, A.; Fonseca, L.; Souza, J.A.; Rivaldo-Gomez, C.; Pomar, C.D.; Criado, D. Anomalous Ferromagnetic Behavior and Size Effects in CuO Nanowires. *J. Magn. Magn. Mater.* **2019**, *471*, 77–81. [CrossRef]
46. Zhan, W.; Chen, Z.; Hu, J.; Chen, X. Vertical CuO Nanowires Array Electrodes: Visible Light Sensitive Photoelectrochemical Biosensor of Ethanol Detection. *Mater. Sci. Semicond. Process.* **2018**, *85*, 90–97. [CrossRef]
47. Mahmoodi, A.; Solaymani, S.; Amini, M.; Nezafat, N.B.; Ghoranneviss, M. Structural, Morphological and Antibacterial Characterization of CuO Nanowires. *Silicon* **2017**, *10*, 1427–1431. [CrossRef]
48. Kim, J.-H.; Katoch, A.; Choi, S.-W.; Kim, S.S. Growth and Sensing Properties of Networked P-CuO Nanowires. *Sens. Actuators B. Chem.* **2015**, *212*, 190–195. [CrossRef]
49. Hadia, N.M.A.; Hajjiah, A.; Elsayed, A.M.; Mohamed, S.H.; Alruqi, M.; Shaban, M.; Alzahrani, F.M.; Abdelazeez, A.A.A.; Rabia, M. Bunch of Grape-Like Shape PANI/Ag_2O/Ag Nanocomposite Photocatalyst for Hydrogen Generation from Wastewater. *Adsorpt. Sci. Technol.* **2022**, *2022*, 4282485. [CrossRef]
50. Sayyah, S.M.; Shaban, M.; Rabia, M. Electropolymerization of *m* -Toluidin on Platinum Electrode from Aqueous Acidic Solution and Character of the Obtained Polymer. *Adv. Polym. Technol.* **2018**, *37*, 126–136. [CrossRef]
51. Sayyah, S.M.; Shaban, M.; Rabia, M. A High-Sensitivity Potentiometric Mercuric Ion Sensor Based on m-Toluidine Films. *IEEE Sens. J.* **2016**, *16*, 1541–1548. [CrossRef]
52. Helmy, A.; Rabia, M.; Shaban, M.; Ashraf, A.M.; Ahmed, S.; Ahmed, A.M. Graphite/Rolled Graphene Oxide/Carbon Nanotube Photoelectrode for Water Splitting of Exhaust Car Solution. *Int. J. Energy Res.* **2020**, *44*, 7687–7697. [CrossRef]

53. Mohamed, H.S.H.; Rabia, M.; Shaban, M.; Taha, S. Controlled Synthesis of CdS Nanoflowers Thin Films for H_2 Electro-Generation. *Mater. Sci. Semicond. Process.* **2020**, *120*, 105307. [CrossRef]
54. Jiang, L.; Zhou, G.; Mi, J.; Wu, Z. Fabrication of Visible-Light-Driven One-Dimensional Anatase TiO_2/Ag Heterojunction Plasmonic Photocatalyst. *Catal. Commun.* **2012**, *24*, 48–51. [CrossRef]
55. Sayyah, S.M.; Shaban, M.; Rabia, M. M-Toluidine Polymer Film Coated Platinum Electrode as a pH Sensor by Potentiometric Methods. *Sens. Lett.* **2015**, *13*, 961–966. [CrossRef]
56. Li, Z.; Qu, Y.; He, G.; Humayun, M.; Chen, S.; Jing, L. Enhanced Visible-Light Activities for PEC Water Reduction of CuO Nanoplates by Coupling with Anatase TiO_2 and Mechanism. *Appl. Surf. Sci.* **2015**, *351*, 681–685. [CrossRef]
57. Rabia, M.; Hadia, N.M.A.; Farid, O.M.; Abdelazeez, A.A.A.; Mohamed, S.H.; Shaban, M. Poly(m-Toluidine)/Rolled Graphene Oxide Nanocomposite Photocathode for Hydrogen Generation from Wastewater. *Int. J. Energy Res.* **2022**, *46*, 11943–11956. [CrossRef]
58. Khalafalla, M.A.H.; Hadia, N.M.A.; Elsayed, A.M.; Alruqi, M.; El Malti, W.; Shaban, M.; Rabia, M. ATO/Polyaniline/PbS Nanocomposite as Highly Efficient Photoelectrode for Hydrogen Production from Wastewater with Theoretical Study for the Water Splitting. *Adsorpt. Sci. Technol.* **2022**, *2022*, 5628032. [CrossRef]
59. Huang, X.; Zhang, M.; Sun, R.; Long, G.; Liu, Y.; Zhao, W. Enhanced Hydrogen Evolution from CuO_x-C/TiO_2 with Multiple Electron Transport Pathways. *PLoS ONE* **2019**, *14*, e0215339. [CrossRef]
60. Sherman, B.D.; Ashford, D.L.; Lapides, A.M.; Sheridan, M.V.; Wee, K.-R.; Meyer, T.J. Light-Driven Water Splitting with a Molecular Electroassembly-Based Core/Shell Photoanode. *J. Phys. Chem. Lett.* **2015**, *6*, 3213–3217. [CrossRef]
61. Naldoni, A.; Guler, U.; Wang, Z.; Marelli, M.; Malara, F.; Meng, X.; Besteiro, L.V.; Govorov, A.O.; Kildishev, A.V.; Boltasseva, A.; et al. Broadband Hot-Electron Collection for Solar Water Splitting with Plasmonic Titanium Nitride. *Adv. Opt. Mater.* **2017**, *5*, 1601031. [CrossRef]
62. Liu, G.; Karuturi, S.K.; Chen, H.; Wang, D.; Ager, J.W.; Simonov, A.N.; Tricoli, A. Enhancement of the Photoelectrochemical Water Splitting by Perovskite $BiFeO_3$ via Interfacial Engineering. *Sol. Energy* **2020**, *202*, 198–203. [CrossRef]
63. Wang, Z.; Cao, D.; Wen, L.; Xu, R.; Obergfell, M.; Mi, Y.; Zhan, Z.; Nasori, N.; Demsar, J.; Lei, Y. Manipulation of Charge Transfer and Transport in Plasmonic-Ferroelectric Hybrids for Photoelectrochemical Applications. *Nat. Commun.* **2016**, *7*, 10348. [CrossRef] [PubMed]
64. Freeman, E.; Kumar, S.; Thomas, S.R.; Pickering, H.; Fermin, D.J.; Eslava, S. $PrFeO_3$ Photocathodes Prepared Through Spray Pyrolysis. *ChemElectroChem* **2020**, *7*, 1365–1372. [CrossRef]
65. Modibane, K.D.; Waleng, N.J.; Ramohlola, K.E.; Maponya, T.C.; Monama, G.R.; Makgopa, K.; Hato, M.J. Poly(3-Aminobenzoic Acid) Decorated with Cobalt Zeolitic Benzimidazolate Framework for Electrochemical Production of Clean Hydrogen. *Polymers* **2020**, *12*, 1581. [CrossRef]